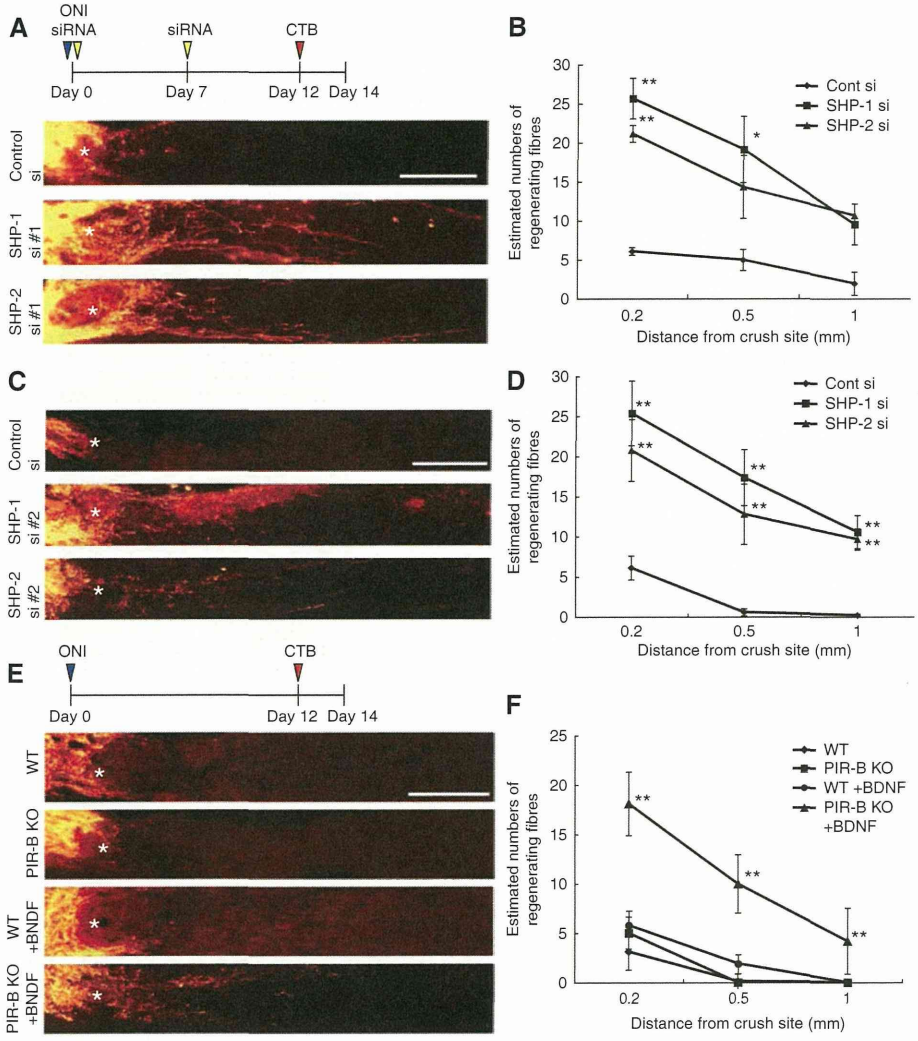

Figure 7 *In vivo* transfection of siRNAs against SHP results in enhanced axonal regeneration. (**A**) Confocal micrographs of optic nerve axons labeled by CTB at 14 days after axotomy. *In vivo* transfection with control siRNA (control si), SHP-1 siRNA #1 (SHP-1 si #1), or SHP-2 siRNA #1 (SHP-2 si #1) was performed. *Injury site. Scale bar: 200 μm. (**B**) Quantitative analysis of regenerating axons extending 0.2, 0.5, and 1.0 mm from the end of the crush site at 14 days after injury. At least five different sections per animal were quantified. Significant differences were found between the control ($N=6$) and the other two groups (SHP-1 si #1 ($N=6$)]and SHP-2 si #1 ($N=7$)). (**C**, **D**) The results were confirmed using different siRNA sets. $N=6$ (control), 7 (SHP-1 siRNA #2 (SHP-1 si #2), and 6 (SHP-2 siRNA #2 (SHP-2 si #2)). (**E**) Longitudinal sections through the optic nerve showing CTB-labeled axons distal to the injury site in WT mice, PIR-B KO mice, and WT mice or PIR-B KO mice treated intravitreally with BDNF 14 days after injury. *Injury site. Scale bar: 200 μm. (**F**) Quantitative analysis of regenerating axons at 14 days after injury. $N=6$ (WT), 6 (PIR-B KO), 6 (WT + BDNF), and 8 (PIR-B KO + BDNF). $^{**}P<0.01$. (**B**, **D**, **F**) $^{*}P<0.05$, $^{**}P<0.01$.

(Kaplan and Miller, 2000; Patapoutian and Reichardt, 2001). Although these signals are activated by binding of neurotrophins to Trk receptors, the basal activity of Trk receptors in the absence of ligand binding may also be important. It has been suggested that SHP-1 is a regulator of basal TrkA activity, because inhibition of endogenous SHP-1 stimulates basal tyrosine phosphorylation of TrkA, thereby promoting the survival of sympathetic neurons and PC12 cells during NGF withdrawal (Marsh *et al*, 2003). Conversely but consistently, our data suggest that the basal Trk receptor activity is reduced by increased binding of SHP-1/2 to Trk receptors, resulting in neurite growth inhibition. This effect may be independent of neurotrophins, because no neurotrophins were added to the culture during the neurite growth assay performed in the present study. Furthermore, BDNF could not be detected in the CGN culture medium (data not shown). Nonetheless, growth of neurites <40 μm in average (Figure 5B and C) may not reflect the crucial role of TrkB in MAG-induced neurite growth inhibition but rather the general importance of TrkB to neurite growth, which cannot be inhibited further.

The SHP family of protein tyrosine phosphatases includes SHP-1, SHP-2, and the *Drosophila melanogaster* homologue Corkscrew (Tonks and Neel, 2001). SHP-1 is expressed in the haematopoietic system, the nervous system, epithelial cells, and the NGF-responsive PC12 cell line (Tonks and Neel, 2001). SHP-1 has been shown to interact with and dephosphorylate several growth factor receptors, including IGF-1, PDGF, EGF (Tonks and Neel, 2001), and TrkA (Marsh *et al*, 2003). It has been shown that SHP-1 acts as a TrkA phosphatase in PC12 cells and sympathetic neurons *in vitro* and *in vivo* and that it maintains low levels of basal TrkA activation and attenuates long-term TrkA signaling in the presence of NGF (Marsh *et al*, 2003). Further, an enhanced

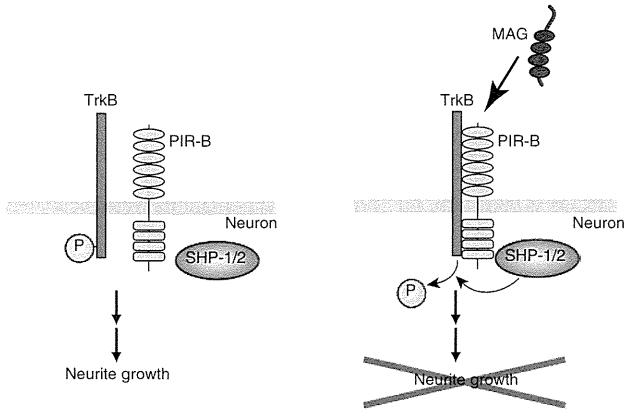

Figure 8 Proposed molecular model of the PIR-B signal transduction. Ligand binding to PIR-B leads to the formation of a receptor complex composed of PIR-B and TrkB. SHP-1/2, which is recruited to PIR-B, interacts with and deactivates TrkB by tyrosine dephosphorylation, causing neurite outgrowth inhibition.

association of SHP-2 with TrkB inhibits BDNF-induced TrkB autophosphorylation and activation in postnatal CGNs (Rusanescu *et al*, 2005). Considering that SHP-1 and SHP-2 negatively regulate Trk activity, the balancing mechanism between Trk receptors and PIR-B may determine the potential of axonal regeneration of the injured CNS through SHP-1 and SHP-2. Further, our observation may be relevant to the development of the nervous system if activation of the basal and/or neurotrophin-dependent Trk activities through PIR-B inhibition contributes to extension of the critical period.

NgR is another receptor for MAG, Nogo, and OMgp. The combination of NgR-null cerebellar neurons and function-blocking PIR-B antibodies has been reported to completely overcome inhibition by myelin (Atwal *et al*, 2008). This implies that the putative third receptor has no role in transducing signals mediated by myelin. It would be interesting to assess the possible cross talk of the downstream signals mediated by PIR-B and NgR. The small guanine nucleoside triphosphatase RhoA has been previously shown to act downstream of NgR as a key intracellular effector of neurite growth inhibition induced by myelin (Yiu and He, 2006). In its active GTP-bound form, RhoA rigidifies the actin cytoskeleton, thereby inhibiting axonal elongation and mediating growth cone collapse. RhoA, which is activated by these proteins, inhibits neurite outgrowth from the postnatal sensory neurons and CGNs (Yiu and He, 2006). In addition, conventional protein kinase C and the EGF receptor are also involved in the inhibitory effect (Yiu and He, 2006). These multiple signals are found downstream of NgR, and they are responsible for the effect of myelin-derived inhibitors. Interestingly, our present data show that inhibition of SHP-1/2 totally abolished the inhibitory effects of MAG on neurons (dephosphorylation of Trk receptors and neurite growth inhibition by MAG–Fc), whereas the inhibition of PIR-B partially reduced the effects. Thus, SHP may be required not only for PIR-B signaling but also for NgR signaling.

Importantly, our data show that inhibition of SHP signaling enhanced axonal regeneration in the injured optic nerve in mice, yet the number of regenerating axons in the optic nerve was fairly reduced. Therefore, SHP may be a new molecular target for treating CNS injuries. Recently, it has been shown that triple-mutant mice that lack MAG, Nogo, and OMgp fail to exhibit any enhancement in the regeneration or functional recovery after spinal cord injury in comparison with WT mice (Lee *et al*, 2010). This report suggests that inhibition of the three myelin inhibitors may be insufficient for axonal regeneration in the CNS. Furthermore, we observed no enhancement in axonal regeneration after spinal cord injury in PIR-B$^{-/-}$ mice (Nakamura *et al*, 2011). However, it should be noted that targeting conventional protein kinase C and the EGF receptor as well as RhoA/Rho-kinase promotes axonal regeneration in the injured CNS (Yiu and He, 2006), which is in agreement with our findings on SHP inhibition. One possible explanation for the inconsistency is that the inhibition of SHP or other intracellular signaling molecules may enhance the intrinsic regenerative response *in vivo*, as Trk activity is induced by silencing SHP. Elucidation of the possible cross talk between myelin signaling and the molecular mechanisms underlying the regenerative response may help clarify the seemingly contradictory findings in this field.

In summary, we dissected the PIR-B signaling cascade responsible for neurite growth inhibition in CGNs and demonstrated the involvement of MAG and Trk receptors. Further, we showed that knockdown of SHP-1 and SHP-2 induced axonal regeneration during CNS injury in mice. We suggest SHP-1 and SHP-2 as potential therapeutic targets for nerve regeneration in CNS injury.

Materials and methods

Animals

We purchased C57BL/6J mice from Charles River Laboratories. These mice were bred and maintained in the Institute of Experimental Animal Sciences at the Osaka University Graduate School of Medicine. PIR-B$^{-/-}$ mice were generated as previously described (Ujike *et al*, 2002) and backcrossed to C57BL/6J mice. We used a C57BL/6J mouse strain bearing a targeted disruption of the third exon of the *p75* gene (Lee *et al*, 1992), which was obtained from the Jackson Laboratory (Bar Harbor, Maine). All experimental procedures were approved by the Institutional Committee of the Osaka University.

Reagents and antibodies

The following reagents were used in this study: purified MAG–Fc (25 μg/ml), recombinant BDNF (100 ng/ml; Peprotech, Rocky Hill, NJ, USA), NSC-87877 (50 μM; Calbiochem, San Diego, CA, USA), and K252a (100 nM; Alomone Labs, Jerusalem, Israel). The TAT–TrkA 481–494 (TAT–QGHIIENPQYFSDA), TAT–TrkA 484–497 (TAT–IIENPQYFSDACVH), and TAT-fused control (TAT–HVCAESFYQPNEII) peptides were chemically synthesized (Sigma-Aldrich, St Louis, MO, USA). Stable CHO cell lines secreting human MAG–Fc were provided by Endo M (Kobe University). The cells were cultured in serum-free medium. Conditioned medium was collected after 3 days, and MAG–Fc was purified with protein A Sepharose beads. For immunoprecipitation, western blotting, and immunostaining the following antibodies were used: monoclonal anti-HA (HA-7, 1:5000; Sigma-Aldrich), anti-c-Myc (9E10, 1:1000; Santa Cruz Biotechnology, CA, USA), biotinylated anti-TrkB (1:2500; R&D systems), anti-SHP-1 (1:1000; BD Transduction Laboratories, San Jose, CA, USA), anti-SHP-2 (1:1000, BD Transduction Laboratories), anti-MAG (1:200; Santa Cruz Biotechnology, Millipore), anti-α-tubulin (1:1000; Santa Cruz Biotechnology), and anti-neuronal class III β-tubulin (Tuj1, 1:5000; Covance Laboratories, Inc., Berkeley, CA, USA); polyclonal anti-SHP-1, anti-SHP-2, anti-Trk, anti-TrkB, anti-PIR-B (1:1000; Santa Cruz Biotechnology), anti-phospho TrkB (1:500 Cell Signaling Technology, Danvers, MA, USA), anti-PIR-B (1 mg/ml; R&D systems), and anti-PIR-A/B (1:1000; BD Pharmingen, San Diego, CA, USA); secondary horseradish peroxidase (HRP)-conjugated anti-mouse, anti-rabbit, or anti-rat IgG (Cell Signaling Technology), HRP-conjugated anti-goat IgG (Santa Cruz

Biotechnology), streptavidin-peroxidase (Roche Applied Science, Indianapolis, IN, USA), and Alexa488- or 568-conjugated goat anti-mouse IgG (Molecular Probes, Eugene, OR, USA).

Plasmid constructs and siRNA

Pir-b was subcloned into the pcDNA3.1Zeo(+) vector as previously described (Endo *et al*, 2008). TrkB constructs were provided by Barde YA (Bibel *et al*, 1999). The mammalian expression vectors encoding human TrkA (Addgene plasmid 15002) (Yano *et al*, 2001), human SHP-1 (Addgene plasmid 8572), and human SHP-2 (Addgene plasmid 8381) were all obtained from Addgene (Cambridge, MA, USA). The following siRNAs were used for knockdown experiments: mouse SHP-1 and mouse SHP-2 (ON-TARGETplus SMARTpool; Thermo Fisher Scientific, Dharmacon Products, Lafayette, CO, USA), and mouse NTRK2 (stealth siRNA; Invitrogen). The ON-TARGET plus SMARTpool siRNA is a mixture of four individual siRNA duplexes. Alexa 488-labeled siRNAs were chemically synthesized (Invitrogen) and contained the following sequences: SHP-1 #1-sense AF488 (5′-GACUGUGACAUUGAUAUC CAGAAGA-3′), SHP-1 #1-antisense (5′-UCUUCUGGAUAUCAAUGU CACAGUC-3′), SHP-1 #2-sense AF488 (5′-CAGCAGAAUACAAACUG CGAACAUU-3′), SHP-1 #2-antisense (5′-AAUGUUCGCAGUUUGUAU UCUGCUG-3′), SHP-2 #1-sense AF488 (5′-CCACUUUGGCUGAACUG GUUCAGUA-3′), SHP-2 #1-antisense (5′-UACUGAACCAGUUCAGC CAAAGUGG-3′), SHP-2 #2-sense AF488 (5′-CCUCUGAAAGGUGGU UCCAUGGUCA-3′), and SHP-2 #1-antisense (5′-UGACCAUGGAACC ACCUUUCAGAGG-3′). As mismatch control, single base pair changes were introduced in the SHP-1 and SHP-2 siRNAs.

Cell culture

COS-7 cells were cultured in Dulbecco's modified Eagle's medium (DMEM; Invitrogen) containing 10% fetal bovine serum (FBS). Transient transfection of COS-7 cells was performed using Lipofectamine 2000 (Invitrogen) according to the manufacturer's instructions. The cells were lysed 24–48 h after transfection and used for immunoprecipitation. Primary dissociated cultures of CGNs from P7 mice were prepared as previously reported (Hata *et al*, 2009). In brief, cells were gently dissociated after digestion with 0.25% trypsin (Gibco/Invitrogen, Paisley, UK) and DNaseI (Takara, Shiga, Japan) at 37°C for 15 min. DMEM/F12 containing 10% FBS was added, and the cells were centrifuged at 1000 r.p.m. for 3 min. The neurons were then plated on poly-L-lysine-coated dishes and maintained in DMEM/F12 supplemented with B27 (Invitrogen) at 37°C with 5% CO_2. After 24 h, the medium was replaced with DMEM/F12 containing 0.1% bovine serum albumin (BSA). After 24-h incubation, the neurons were harvested for immunoprecipitation or western blotting. For dissociated retinal cell cultures, P7–P9 mice were used. Eyes were enucleated, and retinas were dissected and incubated at 37°C for 30 min in a digestion solution containing papain (16.5 U/ml; Worthington Biochem., NJ, USA), DNase (0.5 mg/ml; Sigma), and L-cysteine (0.3 g/ml, Sigma) in phosphate-buffered solution (PBS). Cells were then rinsed with DMEM containing 10% FBS and centrifuged at 1000 r.p.m. for 5 min. To remove cell debris, the cell suspension was passed through a cell strainer (70 μm; BD Falcon, Franklin Lakes, NJ). After centrifugation, the supernatant was discarded and the cells were carefully resuspended in DMEM supplemented with B27 (1:50; Invitrogen) or subjected to nucleofection.

Nucleofection

CGNs and retinal neurons were isolated and dissociated from P7 to P9 mice as described above. The cells were washed and resuspended in room temperature Mouse Neuron Nucleofector Solution (Amaxa; Lonza Cologne AG, Cologne, Germany) at a final concentration of 5×10^6 cells per 100 μl. The cell–nucleofector solution complex (100 μl) and the various siRNA duplexes or control non-targeting siRNA (500 pmol) were then gently mixed and transferred into a cuvette, followed by nucleofection using the nucleofector program O-05. Immediately after electroporation, the cells were mixed with 500 μl of pre-warmed DMEM/F12 containing 10% FBS, and the cell suspension was then transferred onto poly-L-lysine-coated dishes. The cells were placed in an incubator for 3 h, after which the medium was replaced by fresh DMEM/F12 containing B27, and the cells were incubated for an additional 48–72 h. The cells were then transferred to serum-free conditions for immunoprecipitation or western blotting, or collected and plated onto poly-L-lysine-coated dishes for the neurite outgrowth assay.

Co-immunoprecipitation

Cells were washed with ice-cold PBS and lysed on ice in lysis buffer containing 50 mM Tris–HCl (pH 7.4), 150 mM NaCl, 0.5–1% NP-40, 10 mM NaF, 1 mM Na_3VO_4, and a protease inhibitor cocktail (Roche Diagnostics K.K., Tokyo, Japan), followed by centrifugation at 4°C at 15 000 r.p.m. for 10 min. The supernatants were incubated with the indicated antibodies for 2 h or overnight at 4°C. Mouse brains were homogenized in lysis buffer containing 50 mM Tris–HCl (pH 7.5), 150 mM NaCl, 1 mM EDTA, 1.0% NP-40, and a protease inhibitor cocktail (Roche Diagnostics KK). The lysates were centrifuged at $17\,000 \times g$ at 4°C for 15 min and incubated with protein G Sepharose at 4°C for 1 h to reduce non-specific binding to the beads. Cleared lysates were collected and incubated with anti-PIR-B antibodies. The immune complexes were collected after incubation for 1 h at 4°C with protein A Sepharose, protein G Sepharose (GE Healthcare, Chalfont St Giles, England), or streptavidin agarose beads (Thermo Scientific) that had been pre-coated with 0.1–0.5% BSA. After washing the beads three times with the lysis buffer, the proteins were eluted by boiling in 25 μl of 2× sample buffer for 5 min and subjected to sodium dodecyl sulphate polyacrylamide gel electrophoresis (SDS–PAGE), followed by western blotting. Where indicated, the cells were treated with 25 μg/ml MAG–Fc or recombinant human IgG–Fc (R&D systems).

Western blotting

Cell lysates were boiled in sample buffer for 5 min. The proteins were separated by SDS–PAGE and transferred onto polyvinylidene difluoride (PVDF) membranes (Millipore). The membrane was blocked with 5% non-fat dry milk in PBS containing 0.05% Tween-20 (PBS-T) and incubated for 1 h at room temperature or overnight at 4°C, with the primary antibody diluted in PBS-T containing 1% non-fat dry milk. After washing in PBS-T, the membrane was incubated with an HRP-conjugated anti-mouse IgG, anti-rabbit IgG antibody (Cell Signaling Technology), or streptavidin–POD (Roche Applied Science). For detection, an ECL chemiluminescence system (GE Healthcare) was used. Signals were detected and quantified using the LAS-3000 image analyzer (Fuji Film, Tokyo, Japan).

RNA extraction, reverse transcription, and real-time PCR

Total RNA was extracted from CGNs with Trizol (Invitrogen) and reverse transcribed using the High-Capacity cDNA Reverse Transcription Kit (Applied Biosystems, Foster City, CA, USA). mRNA expression was determined by real-time PCR using a 7300 fast real-time PCR system (Applied Biosystems). TaqMan assays (Applied Biosystems) were used to quantitate SHP-1 (Mm00469153_m1) and SHP-2 (Mm 00448434_m1) using the TaqMan Gene Expression Master Mix (Applied Biosystems). The relative mRNA expression was calculated after normalization to the expression of glyceraldehyde 3-phosphate dehydrogenase mRNA. The results of cycle threshold values (Ct values) were calculated by the ΔΔCt method to obtain the fold differences.

Neurite outgrowth assay

Neurite outgrowth assay was performed as described previously (Hata *et al*, 2006). In brief, CGNs were left untreated or were treated with MAG–Fc in DMEM/F12 medium for 24 h. Then, cells were fixed with 4% (w/v) paraformaldehyde (PFA) and immunostained with an anti-TuJ1 monoclonal antibody.

Optic nerve injury, in vivo siRNA transfection, and anterograde labeling

Optic nerve injury was performed as previously described in detail (Smith *et al*, 2009). The left optic nerve of P21 mice was exposed intraorbitally and crushed with fine forceps for 10 s at ~1 mm from the optic disc. Then, intravitreal injections were performed with a pulled glass pipette affixed to a Hamilton syringe. Care was taken not to damage the lens. The animals were divided into different experimental conditions: control siRNA, SHP-1 siRNA, SHP-2 siRNA (1.5 μg/μl), BDNF (5 μg/μl), or control (an equivalent volume of PBS). The second injection was administered 1 week after axotomy. On day 12 after axotomy, 1 μl Alexa555-conjugated CTB (2 μg/μl; Invitrogen) was injected into the vitreous with a glass needle. On day 14 after axotomy, the animals received an overdose of anaesthesia followed by perfusion with 4% PFA. The

eyes were enucleated. The lens and the vitreous body were removed, and the remaining eyecup with the nerve segment was post-fixed in 4% PFA for 12 h at 4°C. The eyecups were then dehydrated in 10–30% sucrose overnight at 4°C and immersed in Optimal Cutting Temperature compound (Tissue Tek). Tissues were frozen in dry ice and serial cross sections (16 μm) were prepared using a cryostat and collected on MAS-coated glass slides.

Immunohistochemistry

Cryostat sections were incubated with blocking solution containing 5% BSA and 0.1–0.2% Triton X-100 in PBS for 1 h at room temperature, followed by overnight incubation with the appropriate antibodies at 4°C. Immunoreactivity was visualized using fluorescence-conjugated secondary antibodies. Coverslips were then mounted with mounting medium.

Quantification of axonal regeneration

Images were acquired on a microscope (BX51; Olympus) equipped with a camera (DP71; Olympus) using the DP Controller software (version 3.1.1.267; Olympus). Axonal regeneration was quantified by counting the number of CTB-labeled axons extending 0.2, 0.5, and 1.0 mm from the end of the crush site in five different sections. The cross-sectional width of the nerve was measured at the point at which the counts were taken and was used to calculate the number of axons per millimetre of nerve width. The number of axons per millimetre was then averaged over the five sections. $\sum ad$, the total number of axons extending the distance d in a nerve having a radius of r, was estimated by summing all the sections having a thickness t (16 μm):

$$\sum ad = \pi r^2 \times (\text{average axons/mm})/t$$

Statistical analysis

The data are presented as the mean ± s.e.m. of 3 independent experiments. Statistical analyses were performed using Welch's *t*-test (Figures 1H, 2A, C and D), one-way ANOVA, followed by Scheffe's (Figures 3A–E, 4F, 5A–C, 6C, 7D and F), Holm's (Figures 4A–E, G, H, 5F, G and 6D–F) or Bonferroni's (Figure 7B) multiple comparison test. *P*-values of <0.05 were considered significant.

Acknowledgements

This work was supported by a Grant-in-Aid for Young Scientists (S) from JSPS. We thank Ben Neel (Ontario Cancer Institute and Princess Margaret Hospital) for providing us with the human SHP-1 and SHP-2 constructs, and Raymond Birge (New York University School of Medicine) for providing us with the human TrkA construct. We thank Katsuhiko Hata for technical advice.

Conflict of interest

The authors declare that they have no conflict of interest.

References

Atwal JK, Pinkston-Gosse J, Syken J, Stawicki S, Wu Y, Shatz C, Tessier-Lavigne M (2008) PirB is a functional receptor for myelin inhibitors of axonal regeneration. *Science* **322:** 967–970

Bibel M, Hoppe E, Barde YA (1999) Biochemical and functional interactions between the neurotrophin receptors trk and p75NTR. *EMBO J* **18:** 616–622

Endo S, Sakamoto Y, Kobayashi E, Nakamura A, Takai T (2008) Regulation of cytotoxic T lymphocyte triggering by PIR-B on dendritic cells. *Proc Natl Acad Sci USA* **105:** 14515–14520

Hata K, Fujitani M, Yasuda Y, Doya H, Saito T, Yamagishi S, Mueller BK, Yamashita T (2006) RGMa inhibition promotes axonal growth and recovery after spinal cord injury. *J Cell Biol* **173:** 47–58

Hata K, Kaibuchi K, Inagaki S, Yamashita T (2009) Unc5B associates with LARG to mediate the action of repulsive guidance molecule. *J Cell Biol* **184:** 737–750

Kaplan DR, Miller FD (2000) Neurotrophin signal transduction in the nervous system. *Curr Opin Neurobiol* **10:** 381–391

Lee JK, Geoffroy CG, Chan AF, Tolentino KE, Crawford MJ, Leal MA, Kang B, Zheng B (2010) Assessing spinal axon regeneration and sprouting in Nogo-, MAG-, and OMgp-deficient mice. *Neuron* **66:** 663–670

Lee KF, Li E, Huber LJ, Landis SC, Sharpe AH, Chao MV, Jaenisch R (1992) Targeted mutation of the gene encoding the low affinity NGF receptor p75 leads to deficits in the peripheral sensory nervous system. *Cell* **69:** 737–749

Marsh HN, Dubreuil CI, Quevedo C, Lee A, Majdan M, Walsh GS, Hausdorff S, Said FA, Zoueva O, Kozlowski M, Siminovitch K, Neel BG, Miller FD, Kaplan DR (2003) SHP-1 negatively regulates neuronal survival by functioning as a TrkA phosphatase. *J Cell Biol* **163:** 999–1010

Nakamura Y, Fujita Y, Ueno M, Takai T, Yamashita T (2011) Paired immunoglobulin-like receptor B knockout does not enhance axonal regeneration or locomotor recovery after spinal cord injury. *J Biol Chem* **286:** 1876–1883; PMID: 21087927

Patapoutian A, Reichardt LF (2001) Trk receptors: mediators of neurotrophin action. *Curr Opin Neurobiol* **11:** 272–280

Rusanescu G, Yang W, Bai A, Neel BG, Feig LA (2005) Tyrosine phosphatase SHP-2 is a mediator of activity-dependent neuronal excitotoxicity. *EMBO J* **24:** 305–314

Schwarze SR, Ho A, Vocero-Akbani A, Dowdy SF (1999) *In vivo* protein transduction: delivery of a biologically active protein into the mouse. *Science* **285:** 1569–1572

Smith PD, Sun F, Park KK, Cai B, Wang C, Kuwako K, Martinez-Carrasco I, Connolly L, He Z (2009) SOCS3 deletion promotes optic nerve regeneration *in vivo*. *Neuron* **64:** 617–623

Syken J, Grandpre T, Kanold PO, Shatz CJ (2006) PirB restricts ocular-dominance plasticity in visual cortex. *Science* **313:** 1795–1800

Takai T (2005) Paired immunoglobulin-like receptors and their MHC class I recognition. *Immunology* **115:** 433–440

Tonks NK, Neel BG (2001) Combinatorial control of the specificity of protein tyrosine phosphatases. *Curr Opin Cell Biol* **13:** 182–195

Ujike A, Takeda K, Nakamura A, Ebihara S, Akiyama K, Takai T (2002) Impaired dendritic cell maturation and increased T(H)2 responses in PIR-B(−/−) mice. *Nat Immunol* **3:** 542–548

Wang KC, Kim JA, Sivasankaran R, Segal R, He Z (2002) P75 interacts with the Nogo receptor as a co-receptor for Nogo, MAG and OMgp. *Nature* **420:** 74–78

Yamashita T, Higuchi H, Tohyama M (2002) The p75 receptor transduces the signal from myelin-associated glycoprotein to Rho. *J Cell Biol* **157:** 565–570

Yano H, Lee FS, Kong H, Chuang J, Arevalo J, Perez P, Sung C, Chao MV (2001) Association of Trk neurotrophin receptors with components of the cytoplasmic dynein motor. *J Neurosci* **21:** RC125

Yiu G, He Z (2006) Glial inhibition of CNS axon regeneration. *Nat Rev Neurosci* **7:** 617–627

Zheng B, Atwal J, Ho C, Case L, He XL, Garcia KC, Steward O, Tessier-Lavigne M (2005) Genetic deletion of the Nogo receptor does not reduce neurite inhibition *in vitro* or promote corticospinal tract regeneration *in vivo*. *Proc Natl Acad Sci USA* **102:** 1205–1210

nature medicine

Angiogenesis induced by CNS inflammation promotes neuronal remodeling through vessel-derived prostacyclin

Rieko Muramatsu[1,2], Chisato Takahashi[1,2], Shuzo Miyake[1,2], Harutoshi Fujimura[3], Hideki Mochizuki[2,4] & Toshihide Yamashita[1,2]

Angiogenesis is a prominent feature of central nervous system (CNS) disease and has roles in both the continued promotion of inflammation and the subsequent repair processes. Here we report that prostacyclin (or prostaglandin I_2 (PGI_2)) derived from new vessels promotes axonal remodeling of injured neuronal networks after CNS inflammation. In a localized model of experimental autoimmune encephalomyelitis (EAE), new vessels formed around the inflammatory lesion, followed by sprouting of adjacent corticospinal tract (CST) fibers. These sprouting fibers formed a compensatory motor circuit, leading to recovery of motor function. Capillary endothelial cell–derived prostacyclin bound to its receptor, the type I prostaglandin receptor (IP receptor), on CST neurons, promoting sprouting of CST fibers and contributing to the repair process. Inhibition of prostacyclin receptor signaling impaired motor recovery, whereas the IP receptor agonist iloprost promoted axonal remodeling and motor recovery after the induction of EAE. These findings reveal an important function of angiogenesis in neuronal rewiring and suggest that prostacyclin is a promising molecule for enhancing functional recovery from CNS disease.

CNS inflammation leads to the disruption of intricate neural networks, causing deficits in motor, sensory, cognitive and other functions[1]. However, these deficits are often followed by limited, but substantial, spontaneous recovery, suggesting that plasticity in remnant neuronal networks compensates for lost functions[2]. In multiple sclerosis, immune-mediated axonal damage is responsible for neurological deficits[3,4]. This axonal damage involves focal degeneration of axons with intact myelin sheaths[5]. In the EAE model of multiple sclerosis, a motor function deficit persists because of substantial loss of axons along the CST, a descending motor tract that connects cortical layer V neurons with spinal targets[6,7]. This deficit is frequently followed by partial recovery, which is associated with spontaneous remodeling of CST axons[8]. However, the molecular mechanisms by which restorative neuronal remodeling is promoted are unknown.

Inflammatory mediators have the potential to remodel the vascular network, suggesting that inflammation may promote angiogenesis[9]. Angiogenesis is a prominent feature of several CNS conditions, including multiple sclerosis, brain tumors, epilepsy and stroke[10,11]. Because neovascularization is thought to pathologically contribute to the development of inflammatory disorders, targeting angiogenesis has been considered beneficial in delaying the course of disease[12]. Designing therapies targeting the angiogenic process is problematic because new blood vessels have roles in wound healing and repair processes, as well as chronic inflammation. Moreover, the vascular niche provides trophic factors for neurons[13]; therefore, new blood vessels induced by inflammation may affect neuronal function.

Prostacyclin (prostaglandin I_2, PGI_2) is one such trophic factor that is synthesized by vascular endothelial and smooth muscle cells[14]. Prostacyclin also inhibits platelet aggregation and is a potent vasodilator[14]. In the present study, we show that prostacyclin derived from new vessels enhances axonal remodeling and promotes functional recovery in EAE.

RESULTS

Compensatory neural circuit formation after localized EAE

We used a localized model of EAE[8,15], which is characterized by the formation of anatomically defined lesions in the spinal cord. We targeted the inflammatory lesion to the dorsal thoracic spinal cord at thoracic levels 3 and 4 (Th3 and Th4), resulting in injury to the bilateral dorsal CST and other dorsal and lateral tract systems (**Supplementary Fig. 1a**)[2,8,15]. Histological evaluation of the spinal cords revealed severe but single focal inflammatory lesions in these mice (**Supplementary Fig. 1b**) that were characterized by the presence of $CD4^+$ and $CD11b^+$ mononuclear inflammatory cells (**Supplementary Fig. 1c**) and focal demyelination (**Supplementary Fig. 1d**). Anterograde tracing revealed that the dorsal CSTs were disrupted at the level of the lesion, resulting in the disappearance of the CSTs below the level of the lesion (**Supplementary Fig. 1e**). Severe hindlimb paresis was followed by partial spontaneous recovery up to day 21 after induction (**Supplementary Fig. 1f**). The hindlimb-placing response, which strongly depends on corticospinal tract integrity, showed a similar pattern of recovery (**Supplementary Fig. 1g**).

[1]Department of Molecular Neuroscience, Graduate School of Medicine, Osaka University, Suita, Osaka, Japan. [2]Japan Science and Technology Agency, Core Research for Evolutional Science and Technology, Tokyo, Japan. [3]Toneyama National Hospital, Toyonaka, Osaka, Japan. [4]Department of Neurology, Graduate School of Medicine, Osaka University, Suita, Osaka, Japan. Correspondence should be addressed to T.Y. (yamashita@molneu.med.osaka-u.ac.jp).

Received 31 May; accepted 17 August; published online 7 October 2012; doi:10.1038/nm.2943

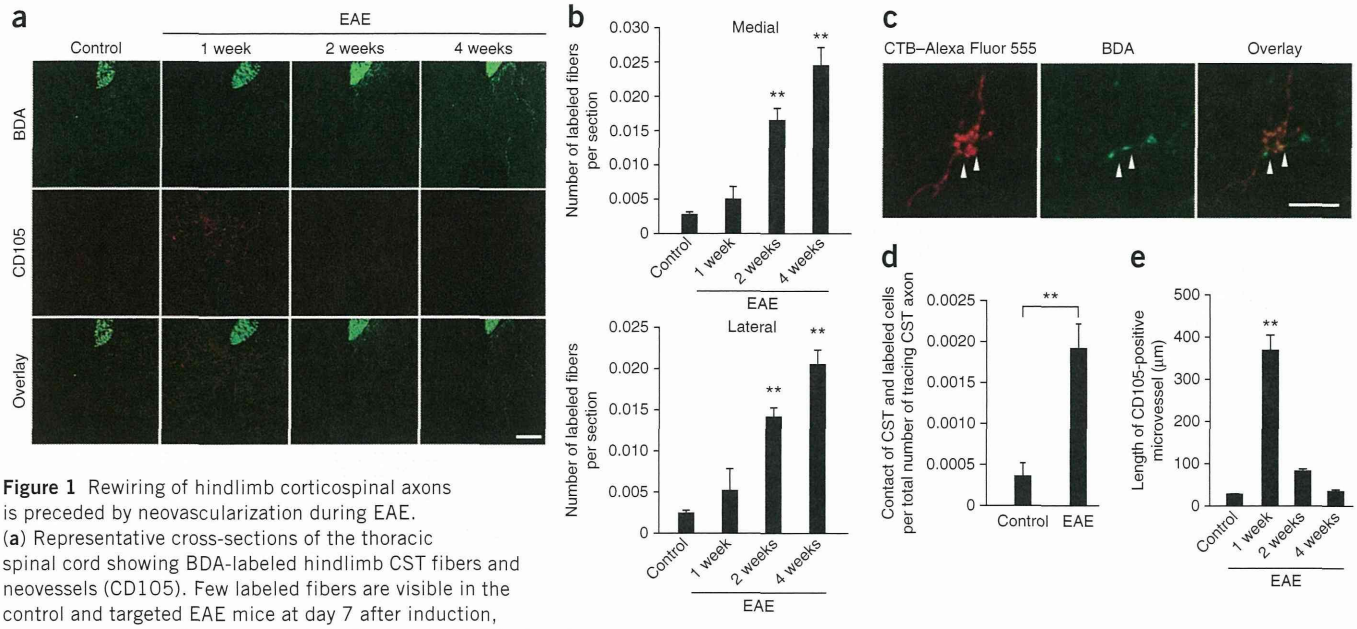

Figure 1 Rewiring of hindlimb corticospinal axons is preceded by neovascularization during EAE. (**a**) Representative cross-sections of the thoracic spinal cord showing BDA-labeled hindlimb CST fibers and neovessels (CD105). Few labeled fibers are visible in the control and targeted EAE mice at day 7 after induction, whereas numerous fibers are visible in the targeted EAE mice at days 14 and 28. Expression of CD105 (marker for proliferating endothelial cells) was induced on day 7. Scale bar, 100 μm. (**b**) Quantitative analysis of the thoracic spinal cord innervations of hindlimb CST fibers. Values represent the mean ± s.e.m. (control: $n = 7$; EAE day 7: $n = 6$; EAE day 14: $n = 6$; EAE day 28: $n = 6$). $^{**}P < 0.01$ using Scheffe's test. (**c**) Thoracic spinal cord cross-section at day 28 after EAE with anterograde labeling of hindlimb CST (BDA) and retrograde tracing of long propriospinal neurons (Alexa Fluor 555–conjugated CTB). Arrowheads indicate the contact positions. Scale bar, 20 μm. (**d**) Quantitative analysis of the contact between labeled CST collaterals and long propriospinal neurons. Values represent the mean ± s.e.m. ($n = 6$ per group). $^{**}P < 0.01$ using Student's t test. (**e**) Quantitative analysis of **a** showing that the length of CD105-positive blood vessels per section (control: $n = 7$; EAE day 7: $n = 6$; EAE day 14: $n = 6$; EAE day 28: $n = 6$). $^{**}P < 0.01$ using Scheffe's test.

Because the recovery of hindlimb motor performance is thought to be caused partly by reorganization of the damaged CST[2,8,15], we further analyzed the events caused by targeted EAE. Although we found only a few biotinylated dextran amine (BDA)-labeled sprouting fibers of the hindlimb CSTs in the thoracic spinal cords of non-EAE control mice (number of collaterals per section: medial, 0.0027; lateral, 0.0024), the number of labeled sprouting fibers in the spinal cords of EAE mice one segment above the lesion increased at 14 and 28 d after lesion (collaterals per section at 14 d: medial, 0.0165; lateral, 0.0142; 28 d: medial, 0.0245; lateral, 0.0205; **Fig. 1a,b** and **Supplementary Fig. 1h,i**). This increase did not start until 7 d after the lesion was induced (collaterals per section at 7 d: medial, 0.0049; lateral, 0.0051; **Fig. 1a,b**). We hypothesized that these sprouting fibers formed a compensatory neuronal network by making functional connections with propriospinal neurons that project intersegmentally to the motor neurons, as has been demonstrated previously after thoracic spinal cord injury[16–18]. To label thoracic propriospinal neurons, we injected Alexa Fluor 555–conjugated cholera toxin subunit B (CTB; a retrograde tracer) into the gray matter of the spinal cords at lumbar levels 1 and 2 (L1 and L2) of control and EAE mice. Two weeks after tracer injection, the number of contacts between BDA-labeled CST collaterals and the cell bodies of the propriospinal neurons labeled with CTB in the spinal cord one segment above the lesion were increased compared with control mice (number of contacts between the CST and CTB-labeled cells: EAE, 0.0025; control, 0.0004; **Fig. 1c,d**).

To test the role of thoracic propriospinal neurons above the lesion in mediating functional recovery, we ablated these neurons by infusing *N*-methyl-D-aspartic acid (NMDA) into the gray matter in the segment above the targeted lesion. Motor function recovered over the course of 28 d after EAE induction. However, 3 d after the infusion of NMDA into EAE mice, hindlimb-placing scores and motor recovery were impaired, as compared to control mice without EAE that had received an infusion of NMDA (**Supplementary Fig. 2a,b**). The reductions in number of neurons, amount of myelin and lesion length in the spinal cord induced by NMDA injection were comparable between EAE and control mice (**Supplementary Fig. 2c–h**). These results show that the CST collaterals formed new connections with the lumbar spinal cord through the propriospinal pathway. The time course of this reorganization is associated closely with that of motor recovery after EAE induction. Thus, these findings provide an anatomical basis for the recovery of motor function and neuronal remodeling during the course of targeted EAE.

Angiogenesis precedes CST reorganization

During the development of the nervous system, axons are guided by attractive and repulsive cues in the extracellular matrix[19]. However, the neuronal network formed as a result of EAE differs from the developmentally formed locomotor network, suggesting that the molecules and mechanisms involved may also differ[2]. Inflammatory processes in several diseases can induce angiogenesis[20]. Thus, we measured the extent of new vessel formation by immunostaining for CD105 (endoglin), a marker of angiogenesis that is expressed in the brains of patients with multiple sclerosis[21]. Seven days after the induction of EAE, the length of CD105-positive capillaries increased markedly around the focal lesions in the spinal cords of EAE mice (368.5 μm per section) compared with control mice (28.2 μm per section; **Fig. 1a,e** and **Supplementary Fig. 3a**) and then decreased to the baseline level and remained there at 2 weeks after induction. The lengths of CD31 (PECAM-1)-positive endothelial cells increased in the inflammatory lesions at 1 week after EAE induction and remained elevated for up to 4 weeks (**Supplementary Fig. 3b,c**). We observed colocalization of CD105 with some of the CD31-positive

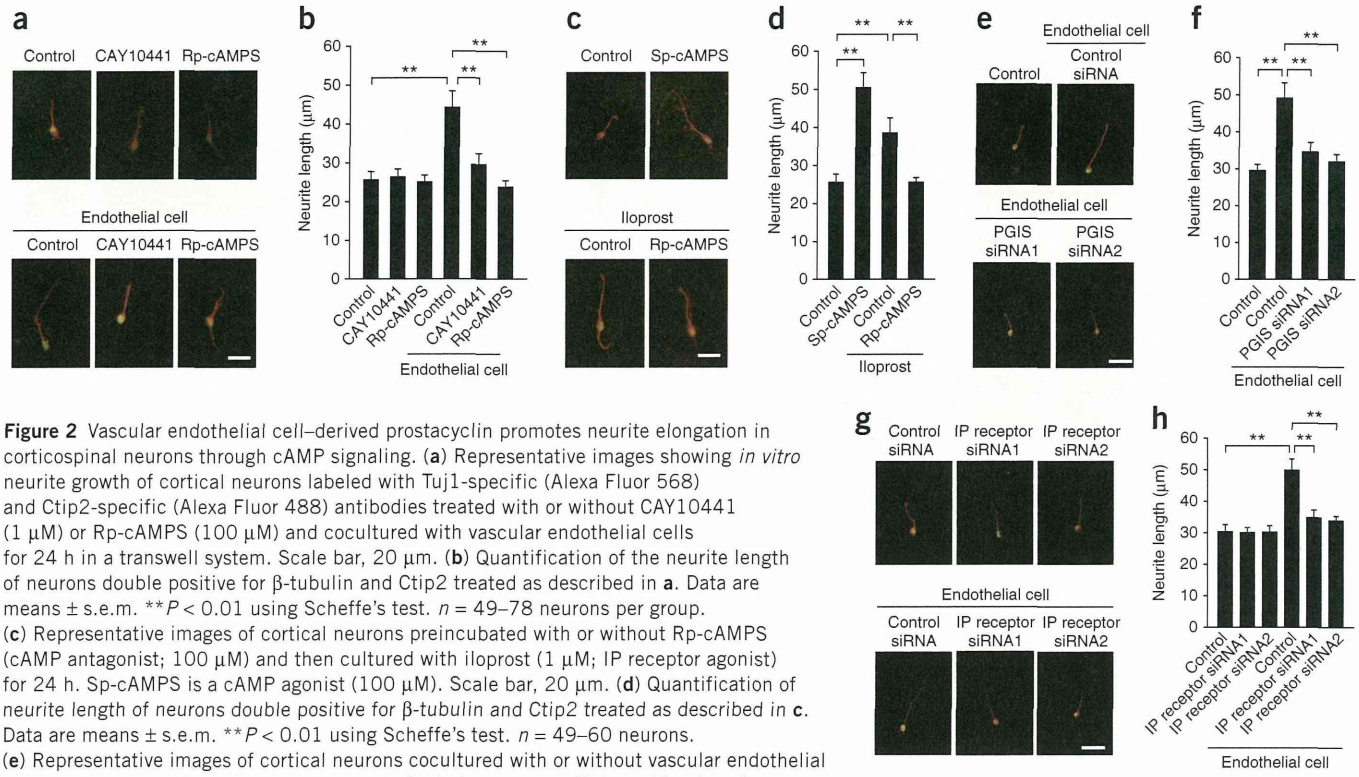

Figure 2 Vascular endothelial cell–derived prostacyclin promotes neurite elongation in corticospinal neurons through cAMP signaling. (**a**) Representative images showing *in vitro* neurite growth of cortical neurons labeled with Tuj1-specific (Alexa Fluor 568) and Ctip2-specific (Alexa Fluor 488) antibodies treated with or without CAY10441 (1 μM) or Rp-cAMPS (100 μM) and cocultured with vascular endothelial cells for 24 h in a transwell system. Scale bar, 20 μm. (**b**) Quantification of the neurite length of neurons double positive for β-tubulin and Ctip2 treated as described in **a**. Data are means ± s.e.m. $^{**}P < 0.01$ using Scheffe's test. $n = 49$–78 neurons per group. (**c**) Representative images of cortical neurons preincubated with or without Rp-cAMPS (cAMP antagonist; 100 μM) and then cultured with iloprost (1 μM; IP receptor agonist) for 24 h. Sp-cAMPS is a cAMP agonist (100 μM). Scale bar, 20 μm. (**d**) Quantification of neurite length of neurons double positive for β-tubulin and Ctip2 treated as described in **c**. Data are means ± s.e.m. $^{**}P < 0.01$ using Scheffe's test. $n = 49$–60 neurons. (**e**) Representative images of cortical neurons cocultured with or without vascular endothelial cells that were transfected with PGIS siRNA. Scale bar, 20 μm. (**f**) Quantification of neurite length of the neurons double positive for β-tubulin and Ctip2 treated as described in **e**. Data are means ± s.e.m. $^{**}P < 0.01$ using Scheffe's test. $n = 36$–82 neurons. (**g**) Representative images of cortical neurons transfected with IP receptor siRNA or control siRNA and cocultured with vascular endothelial cells. Scale bar, 20 μm. (**h**) Quantification of neurite length of the neurons double positive for β-tubulin and Ctip2 treated as described in **g**. Data are means ± s.e.m. $^{**}P < 0.01$ using Scheffe's test. $n = 50$–65 neurons.

endothelial cells (**Supplementary Fig. 3d**). We used CD105 as a marker for angiogenesis because it was coexpressed with Ki67 in capillaries (**Supplementary Fig. 3e**). These results suggest that the increase in the density of vascular endothelial cells was caused by the increase in the density of the new vessels. The kinetics of these findings reveal that new vessel formation was followed by reorganization of the CST.

Prostacyclin promotes axonal elongation

The results described above prompted us to investigate whether the newly formed blood vessels secrete factors that promote axonal sprouting, resulting in reorganization of the neuronal network. Therefore, we next explored whether vascular endothelial cells promote neurite growth *in vitro*. We prepared vascular endothelial cells and cortical neurons from mouse brains and cocultured them in a transwell system for 24 h to prevent contact between the different cell types and measured neurite length of neurons that were positive for Tuj1, a class III β-tubulin, and COUP transcription factor interacting protein 2 (Ctip2, also known as Bcl11B), a marker of subcortically projecting neurons including those in the CST. Notably, neurite length increased when cocultured with vascular endothelial cells as compared with control neurons cultured without endothelial cells (control, 27.91 μm; coculture, 45.26 μm; **Fig. 2a,b**). These results suggest that a diffusible factor or factors secreted from brain endothelial cells may promote neurite outgrowth in corticospinal neurons.

To identify the soluble factor(s) responsible for this effect, we focused on vasoconstrictor peptides, including endothelin[22]. By ELISA, we detected a stable metabolite of prostacyclin, 6-keto prostaglandin F1 α (6-keto–PGF1-α) in the medium of cultured endothelial cells (20.6 ng per ml in 10^6 cells) from control mice after 1 d *in vitro*. We did not detect 6-keto–PGF1-α in the supernatants from cultures of cortical neurons (data not shown). The prostacyclin receptor (IP receptor) is a G protein–coupled receptor that is primarily coupled to the activation of adenylate cyclase, which catalyzes the formation of 3′,5′ cyclic adenosine monophosphate (cAMP)[14], a key messenger for axon regeneration[23,24]. Treatment of neurons with the IP receptor antagonist CAY10441 abrogated the effect of endothelial cells on neurite growth (coculture, 45.26 μm; CAY10441, 30.71 μm; **Fig. 2a,b**). These results suggest that vascular endothelial cells promote neurite elongation through the IP receptor.

Because the binding of prostacyclin to the IP receptor increases the amount of cAMP, we investigated whether the elevation in intracellular cAMP in neurons was required for neurite elongation. We found that treatment of neurons with Rp-cAMPS, an antagonist of cAMP, inhibited endothelial cell–induced neurite elongation (coculture, 45.26 μm; Rp-cAMPS, 26.84 μm; **Fig. 2a,b**). Conversely, treatment of neurons with iloprost, an IP receptor agonist, promoted neurite elongation in a cAMP-dependent manner (vehicle-treated control, 27.91 μm; iloprost, 42.14 μm; iloprost and Rp-cAMPS, 26.90 μm; **Fig. 2c,d**). We confirmed that treatment with Sp-cAMPS, an agonist of cAMP, enhanced neurite elongation (vehicle-treated control, 27.91 μm; iloprost, 50.45 μm; **Fig. 2c,d**).

To assess whether prostacyclin released from vascular endothelial cells was responsible for the observed effect on neurite elongation, we transfected endothelial cells with two different prostacyclin synthase (PGIS) siRNAs, siRNA1 and siRNA2 (**Supplementary Fig. 4a**)

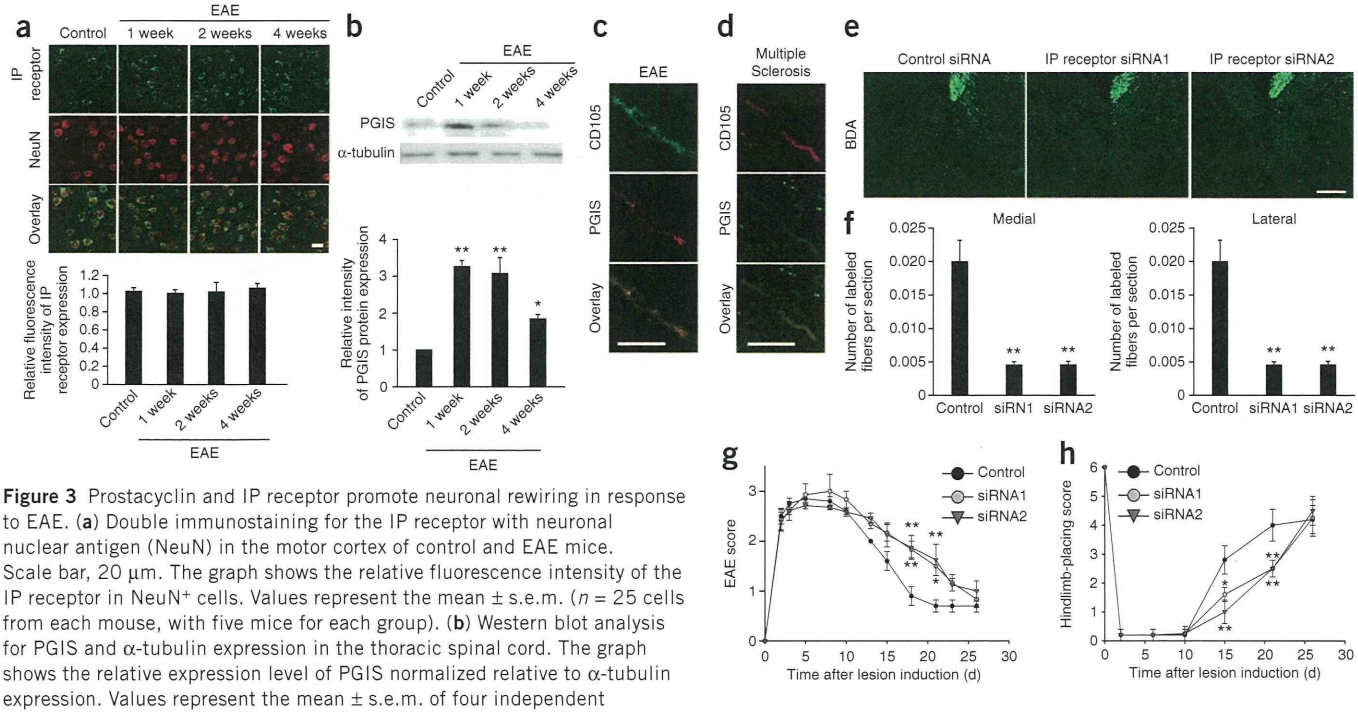

Figure 3 Prostacyclin and IP receptor promote neuronal rewiring in response to EAE. (**a**) Double immunostaining for the IP receptor with neuronal nuclear antigen (NeuN) in the motor cortex of control and EAE mice. Scale bar, 20 μm. The graph shows the relative fluorescence intensity of the IP receptor in NeuN$^+$ cells. Values represent the mean ± s.e.m. (n = 25 cells from each mouse, with five mice for each group). (**b**) Western blot analysis for PGIS and α-tubulin expression in the thoracic spinal cord. The graph shows the relative expression level of PGIS normalized relative to α-tubulin expression. Values represent the mean ± s.e.m. of four independent experiments. $*P < 0.05$, $**P < 0.01$ using one-way analysis of variance (ANOVA) followed by Tukey's test. (**c**) Immunostaining for PGIS and CD105 in the spinal cord after EAE. Scale bar, 10 μm. (**d**) Immunostaining for CD105 and PGIS in autopsy spinal cord samples from individuals with multiple sclerosis. Scale bar, 10 μm. (**e**) Representative sections of the thoracic spinal cord showing BDA-labeled sprouting fibers of the CST 14 d after EAE induction. Scale bar, 100 μm. (**f**) Quantitative analysis of hindlimb CST fiber innervation in the thoracic spinal cord 14 d after EAE induction. $**P < 0.01$ using one-way ANOVA followed by Scheffe's test. Values are represented as mean ± s.e.m. (control: n = 7; IP receptor siRNA1: n = 6; IP receptor siRNA2: n = 6). (**g**,**h**) Quantification of EAE scores (**g**) and hindlimb-placing scores (**h**) in EAE mice treated with control siRNA or siRNA directed against the IP receptor (siRNA1 and siRNA2). Values are represented as mean ± s.e.m. $*P < 0.05$, $**P < 0.01$ using one-way ANOVA followed by Bonferroni's test.

and found that, when these were cocultured with neurons, silencing of PGIS inhibited neurite elongation (control siRNA, 49.07 μm; PGIS siRNA1, 34.55 μm; PGIS siRNA2, 31.91 μm; **Fig. 2e**,**f**). When we knocked down IP receptor expression in the cortical neurons (**Supplementary Fig. 4b**), vascular endothelial cell–induced neurite elongation was completely inhibited (control siRNA, 49.81 μm; IP receptor siRNA1, 34.79 μm; IP receptor siRNA2, 33.78 μm; **Fig. 2g**,**h**). Therefore, prostacyclin derived from vascular endothelial cells promotes neurite outgrowth of corticospinal neurons *in vitro* through the IP receptor and activation of adenylate cyclase.

The IP receptor is crucial for motor recovery from EAE

We investigated whether prostacyclin signaling promotes neuronal remodeling and motor recovery in EAE mice. Immunohistochemical analysis revealed that the majority of the neurons in layer V of the hindlimb motor cortex expressed IP receptor before and after the induction of EAE (**Fig. 3a**). Glial fibrillary acidic protein (GFAP)-positive astrocytes in the motor cortex expressed the IP receptor at very low levels (**Supplementary Fig. 5a**). We found an increase in PGIS and 6-keto–PGF1-α expression in the lesioned tissues (**Fig. 3b** and **Supplementary Fig. 5b**), with expression of PGIS primarily in the CD105-positive neovessels (**Fig. 3c**) but not in neurons or astrocytes in the spinal cord (**Supplementary Fig. 5c**). Although PGIS was also expressed in CD31$^+$ as well as in platelet-derived growth factor receptor-α (PDGFR-α)-positive cells in the spinal cord, the levels of their expressions in each cell were unchanged on day 7 after the induction of EAE (**Supplementary Fig. 5c**,**d**). The level of PGIS in CD31$^+$ vascular endothelial cells was comparable between control and EAE spinal cords (**Supplementary Fig. 5e**), suggesting that the increase in PGIS expression after EAE induction was caused by the increase in neovessel formation and the upregulation of PGIS in these vessels. Moreover, we observed weak expression of cyclooxygenase 2 (COX-2) in the focal EAE lesions of the spinal cord (**Supplementary Fig. 5f**). We also detected PGIS expression in CD105-positive cells in brain and spinal cord autopsy samples obtained from three individuals with multiple sclerosis (**Fig. 3d**).

To investigate whether the activation of IP receptor is required for motor recovery from EAE-induced paresis, we knocked down expression of the IP receptor *in vivo* by transfecting neurons in layer V of the hindlimb motor cortices with IP receptor siRNA1 or siRNA2 in EAE mice (**Supplementary Fig. 6a–d**). This enabled us to specifically block the IP receptor in CST neurons while investigating the effects in the spinal cord. *In vivo* transfection of IP receptor siRNAs decreased the formation of CST collaterals in response to focal EAE lesions (IP receptor siRNA1: medial, 0.0045; lateral, 0.0042; IP receptor siRNA2: medial, 0.0045; lateral, 0.0043) compared with control siRNA transfection at 14 d after induction of EAE (control siRNA: medial, 0.0200; lateral, 0.0190; **Fig. 3e**,**f** and **Supplementary Fig. 6e**). Spontaneous recovery of motor function was delayed by knockdown of the IP receptor by siRNA (**Fig. 3g**,**h**). This effect of IP receptor knockdown on axonal remodeling was not caused by increased dieback of the CST, which is immunoreactive for protein kinase C γ (PKC-γ, a marker of the CST), rostral to the lesion (**Supplementary Fig. 6f**,**g**). Of note, in the cervical spinal cord, a location distal to the lesion, the formation of CST collaterals increased in EAE, and this increase was not abolished by transfection of IP receptor siRNA

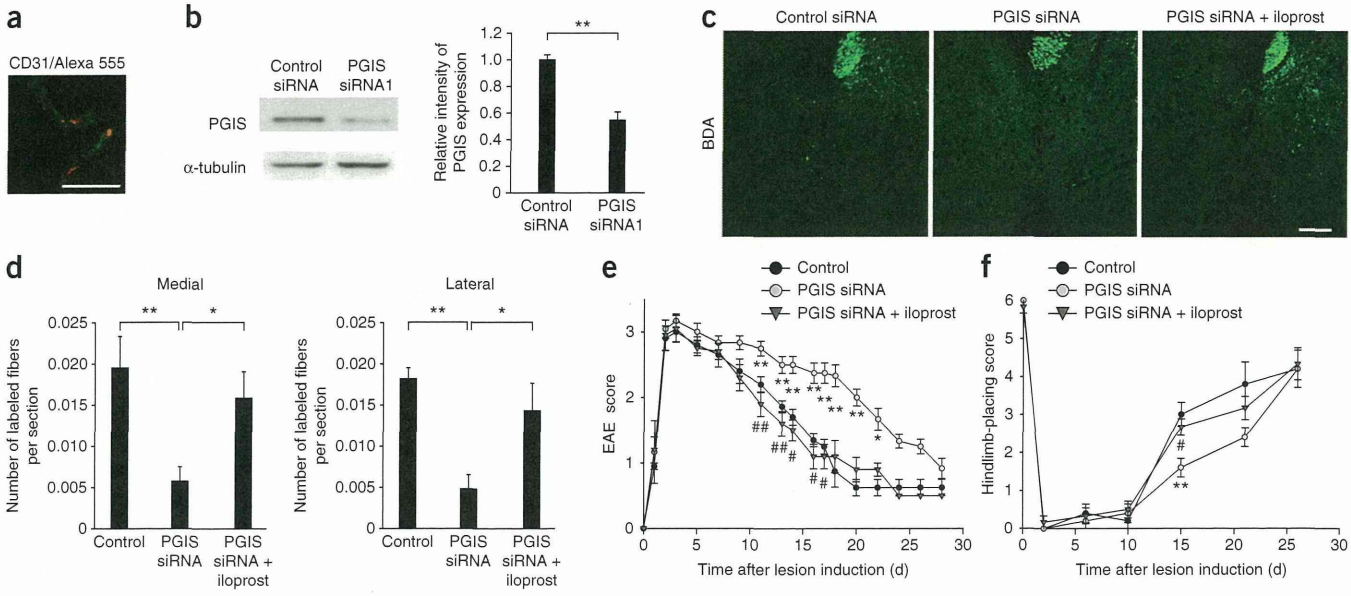

Figure 4 Knockdown of PGIS in vascular endothelial cells delays recovery of motor function in EAE. (**a**) Representative image of a brain section immunostained for CD31 (Alexa Fluor 488) in mice transfected with Alexa Fluor 555–labeled oligonucleotides showing that transfection of the oligonucleotide into the endothelial cells succeeded *in vivo*. Scale bar, 20 μm. (**b**) Expression of PGIS in capillary endothelial cells in the brain after transfection with PGIS siRNA. The graph shows the relative intensity of the PGIS bands relative to α-tubulin. Values are represented as mean ± s.e.m. $^{**}P < 0.01$ using one-way ANOVA followed by Student's *t* test. (**c**) Representative cross-sections of the thoracic spinal cord showing BDA-labeled sprouting fibers of the CST 14 d after the induction of EAE. Scale bar, 100 μm. (**d**) Quantitative analysis of hindlimb CST fiber innervation in the thoracic spinal cord 14 d after EAE induction. Values represent the mean ± s.e.m. (control: $n = 5$; PGIS siRNA: $n = 7$; PGIS siRNA plus iloprost: $n = 6$). $^{*}P < 0.05$, $^{**}P < 0.01$ using one-way ANOVA followed by Scheffe's test. (**e**,**f**) Quantification of EAE scores (**e**) and hindlimb-placing scores (**f**) in EAE mice treated as indicated. Values are represented as mean ± s.e.m. (control siRNA: $n = 6$; PGIS siRNA: $n = 6$; PGIS siRNA plus iloprost: $n = 6$). $^{*}P < 0.05$, $^{**}P < 0.01$ compared to control, $^{\#}P < 0.05$, $^{\#\#}P < 0.01$ compared to PGIS siRNA using one-way ANOVA followed by Bonferroni's test.

(**Supplementary Fig. 6h**,**i**), suggesting these plastic changes in CST remodeling in this remote area are induced through a mechanism that is independent of the IP receptor. These results suggest the IP receptor is required for CST reorganization around the EAE lesion, as well as for one phase of functional recovery after induction of focal EAE.

Prostacyclin drives motor recovery and CST reorganization

To assess the role of prostacyclin expressed in vascular endothelial cells, we inhibited PGIS expression in vascular endothelial cells (**Fig. 4a**,**b**) by intravenous injection of PGIS siRNA. This procedure achieved selective suppression of PGIS expression in $CD31^+$ cells but not in PDGFR-α^+ cells in the spinal cord (**Supplementary Fig. 7a**,**b**). Indeed, we did not observe the transfected fluorescent oligonucleotide in PDGFR-α^+–cells (**Supplementary Fig. 7c**). CST collateral formation was reduced on day 14 after EAE induction when endothelial vascular cells were transfected with PGIS siRNA at days 0 and 7 (medial, 0.0058; lateral, 0.0048) as compared to transfection of EAE mice with the control siRNA (medial, 0.0200; lateral, 0.0182; **Fig. 4c**,**d** and **Supplementary Fig. 7d**). Recovery of motor function was delayed by PGIS knockdown in endothelial cells (**Fig. 4e**,**f**). The effect of PGIS knockdown on CST reorganization and recovery of motor function was attenuated by intrathecal treatment with the IP receptor agonist iloprost on the day after EAE induction (PGIS siRNA: medial, 0.0058; lateral, 0.0048; PGIS siRNA plus iloprost: medial, 0.0159; lateral, 0.0143; **Fig. 4c–f**). None of the treatments (PGIS siRNA or iloprost) affected vascular formation compared to EAE plus control siRNA in the spinal cord (**Supplementary Fig. 7e**,**f**). These data show that prostacyclin expressed by vascular endothelial cells is required for reorganization of the CST and functional recovery after EAE.

IP receptor agonist promotes motor recovery

We next tested whether IP receptor activation promoted recovery after EAE. We delivered iloprost intrathecally into the thoracic spinal cord using osmotic minipumps starting on the day of EAE induction. Treatment with iloprost significantly increased the number of BDA-labeled sprouting CST fibers at day 14 after induction (medial, 0.0243; lateral, 0.0230) compared to treatment with a vehicle control (medial, 0.0172; lateral, 0.0158; **Fig. 5a**,**b** and **Supplementary Fig. 8a**). This treatment did not alter PGIS expression in the lesioned tissues 7 d after EAE induction (**Fig. 5c**). EAE scores and spontaneous recovery of motor function were accelerated by iloprost treatment (**Fig. 5d**,**e**).

To obtain additional electrophysiological evidence regarding rewiring of the injured CST, we measured cortical-evoked cord dorsum potentials (CDPs) at 14 d after induction of EAE. The results showed that the connection from the cerebral cortex to the CST below the EAE lesion was facilitated by iloprost treatment (**Fig. 5f**,**g**). Consistent with the siRNA results, treatment with CAY10441, an IP receptor antagonist, significantly decreased the number of BDA-labeled sprouting CST fibers at 14 d after EAE induction (medial, 0.0063; lateral, 0.0063) compared to treatment with the vehicle control (**Fig. 5a**,**b**). Spontaneous recovery of motor function and reconnection of the injured CST as measured by CDPs were also prevented by treatment with CAY10441 (**Fig. 5d–g**). Oligodendrocytes in the spinal cord only faintly expressed the IP receptor (**Supplementary Fig. 8b**). Neither iloprost nor CAY10441 had an effect on myelination, axonal damage or the formation of new vessels in the spinal cord at 14 d after EAE induction (**Supplementary Fig. 8c–f**) and did not alter the accumulation of $CD4^+$ or $CD11b^+$ cells in the spinal cord at 7 d after induction (**Supplementary Fig. 8c**,**d**).

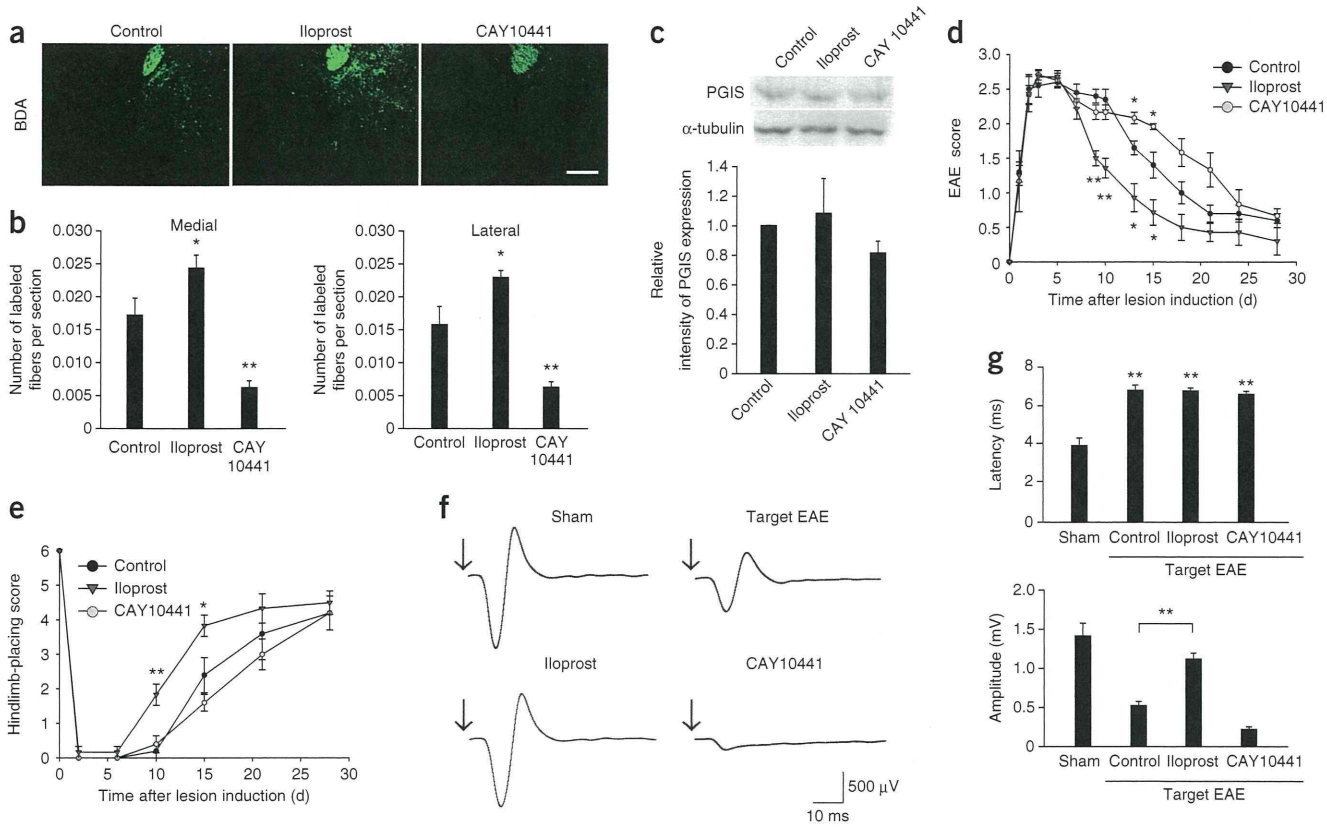

Figure 5 Treatment with iloprost improves the EAE-induced deficit in motor function. (**a**) Representative cross-sections of the thoracic spinal cord showing BDA-labeled sprouting fibers of the CST 14 d after the induction of EAE and treatment with iloprost or CAY10441. Scale bar, 100 µm. (**b**) Quantitative analysis of hindlimb CST fiber innervation in the thoracic spinal cord 14 d after EAE induction. Values are represented as mean ± s.e.m. (control: $n = 6$; iloprost: $n = 5$; CAY10441: $n = 6$). $^{*}P < 0.05$, $^{**}P < 0.01$ using one-way ANOVA followed by Scheffe's test. (**c**) Western blot analysis and relative quantification of PGIS expression in target lesions of the thoracic spinal cord obtained from each group of mice. Values are represented as mean ± s.e.m. ($n = 3$). (**d**,**e**) Quantification of EAE scores (**d**) and hindlimb-placing scores (**e**) in EAE mice treated with iloprost or CAY10441. Values are represented as mean ± s.e.m. (control: $n = 6$; iloprost: $n = 5$; CAY10441: $n = 6$). $^{*}P < 0.05$, $^{**}P < 0.01$ using one-way ANOVA followed by Bonferroni's test. (**f**) Representative sample traces of cortical evoked potentials below the lesion in each group of mice. Arrows indicate the times of cortical stimulation. (**g**) The average latencies and amplitudes of cortical evoked potentials from the experiments in **f**. Values are represented as mean ± s.e.m. (sham: $n = 6$, control: $n = 6$; iloprost: $n = 5$; CAY10441: $n = 6$). $^{**}P < 0.01$ using one-way ANOVA followed by Scheffe's test.

Treatment with either iloprost or CAY10441 did not alter T cell responses to antigen in a proliferation assay compared with vehicle-treated controls (**Supplementary Fig. 9a**). Moreover, we observed no differences in the concentration of various cytokines in the spinal cord tissue or the amount secreted by T cells obtained from vehicle-, iloprost- or CAY10441-treated mice stimulated with myelin basic protein (MBP) (**Supplementary Fig. 9b,c**). These results suggest that iloprost or CAY10441 did not affect inflammation.

DISCUSSION

Our present findings suggest that soluble factors released from the vascular endothelium promote axonal rewiring and functional recovery in EAE. Treatment with iloprost does not reduce the clinical onset of EAE in rats[25], suggesting the IP receptor is not involved in the development of EAE and prostacyclin and its receptor do not have a major role in regulating inflammation in EAE. Supporting this notion, our *in vitro* experiments revealed that prostacyclin does not modulate T cell proliferation or cytokine production from re-stimulated T cells *in vitro*. In addition, because prostacyclin is secreted by new vessels, which are formed as a result of inflammation, prostacyclin may act specifically during the remission phase of EAE. In this context, we describe a new role for prostacyclin.

During development, peripheral sympathetic axons are guided by endothelin secreted from the external carotid artery[26], suggesting that axonal guidance is influenced by endothelium-derived factors during development of the peripheral nervous system. In contrast, a close association of axons and blood vessels had not been observed in the CNS, suggesting this type of navigation was PNS specific and restricted to development. Our present findings reveal an unexpected function of blood vessels in the adult CNS in response to injury. Prostacyclin may be associated with other types of CNS disease, as neovascularization also occurs in brain tumors, epilepsy and stroke. *In vivo* imaging has suggested a role of new vessels in influencing sprouting of injured axons in response to spinal cord injury[27]. Blood vessel density is increased within 2 weeks after spinal cord injury, and these vessels seem to exert a growth-stimulating action on dorsal root ganglia[27]. Thus, the mechanism we identified here may be relevant to other CNS diseases that disrupt neuronal networks in adults. Taken together, our *in vitro* and *in vivo* findings show that prostacyclin is secreted from neovessels formed as a result of CNS inflammation. By signaling through the IP receptor expressed on neurons, this promotes neuronal remodeling and the formation of a compensatory motor neuronal network that contributes to the recovery of hindlimb motor function after EAE.

METHODS

Methods and any associated references are available in the online version of the paper.

Note: Supplementary information is available in the online version of the paper.

ACKNOWLEDGMENTS

The authors are grateful to N. Takakura, H. Kidoya and M. Ueno for helpful comments and M. Niwa and S. Nakagawa for technical advice on culturing of endothelial cells. This work was supported by a Grant-in-Aid for Scientific Research on Innovative Areas (23122512) from the Japan Society for the Promotion of Sciences to R.M. and the Core Research for Evolutional Science and Technology from Japan Science and Technology Agency to T.Y.

AUTHOR CONTRIBUTIONS

R.M. performed all experiments, with the exception of the portions indicated below. C.T. supported immunohistochemical analyses. C.T. and S.M. helped with *in vitro* experiments. H.M. and H.F. provided the autopsy samples from individuals with multiple sclerosis. R.M. and T.Y. designed the experiments. T.Y. coordinated and directed the project and wrote the manuscript.

COMPETING FINANCIAL INTERESTS

The authors declare no competing financial interests.

Published online at http://www.nature.com/doifinder/10.1038/nm.2943.
Reprints and permissions information is available online at http://www.nature.com/reprints/index.html.

1. Lucas, S.M., Rothwell, N.J. & Gibson, R.M. The role of inflammation in CNS injury and disease. *Br. J. Pharmacol.* **147**, S232–S240 (2006).
2. Harel, N.Y. & Strittmatter, S.M. Can regenerating axons recapitulate developmental guidance during recovery from spinal cord injury? *Nat. Rev. Neurosci.* **7**, 603–616 (2006).
3. Hauser, S.L. & Oksenberg, J.R. The neurobiology of multiple sclerosis: genes, inflammation, and neurodegeneration. *Neuron* **52**, 61–76 (2006).
4. Trapp, B.D. & Nave, K.A. Multiple sclerosis: an immune or neurodegenerative disorder? *Annu. Rev. Neurosci.* **31**, 247–269 (2008).
5. Nikić, I. *et al.* A reversible form of axon damage in experimental autoimmune encephalomyelitis and multiple sclerosis. *Nat. Med.* **17**, 495–499 (2011).
6. DeLuca, G.C., Ebers, G.C. & Esiri, M.M. Axonal loss in multiple sclerosis: a pathological survey of the corticospinal and sensory tracts. *Brain* **127**, 1009–1018 (2004).
7. Black, J.A., Liu, S., Hains, B.C., Saab, C.Y. & Waxman, S.G. Long-term protection of central axons with phenytoin in monophasic and chronic-relapsing EAE. *Brain* **129**, 3196–3208 (2006).
8. Kerschensteiner, M. *et al.* Remodeling of axonal connections contributes to recovery in an animal model of multiple sclerosis. *J. Exp. Med.* **200**, 1027–1038 (2004).
9. Jackson, J.R., Seed, M.P., Kircher, C.H., Willoughby, D.A. & Winkler, J.D. The codependence of angiogenesis and chronic inflammation. *FASEB J.* **11**, 457–465 (1997).
10. Fokman, J. & Brem, H. Angiogenesis and inflammation. in *Inflammation: Basic Principles and Clinical Correlates.* 2nd edn., 821–839 (Raven Press, New York, 1992).
11. Kirk, S., Frank, J.A. & Karlik, S. Angiogenesis in multiple sclerosis: is it good, bad or an epiphenomenon? *J. Neurol. Sci.* **217**, 125–130 (2004).
12. Costa, C., Incio, J. & Soares, R. Angiogenesis and chronic inflammation: cause or consequence? *Angiogenesis* **10**, 149–166 (2007).
13. Carmeliet, P. Blood vessels and nerves: common signals, pathways and diseases. *Nat. Rev. Genet.* **4**, 710–720 (2003).
14. Vane, J.R. & Botting, R.M. Pharmacodynamic profile of prostacyclin. *Am. J. Cardiol.* **75**, 3A–10A (1995).
15. Buddeberg, B.S. *et al.* Behavioral testing strategies in a localized animal model of multiple sclerosis. *J. Neuroimmunol.* **153**, 158–170 (2004).
16. Bareyre, F.M. *et al.* The injured spinal cord spontaneously forms a new intraspinal circuit in adult rats. *Nat. Neurosci.* **7**, 269–277 (2004).
17. Courtine, G. *et al.* Recovery of supraspinal control of stepping via indirect propriospinal relay connections after spinal cord injury. *Nat. Med.* **14**, 69–74 (2008).
18. Menétrey, D., de Pommery, J. & Roudier, F. Propriospinal fibers reaching the lumber enlargement in the rat. *Neurosci. Lett.* **58**, 257–261 (1985).
19. Tessier-Lavigne, M. & Goodman, C.S. The molecular biology of axon guidance. *Science* **274**, 1123–1133 (1996).
20. Kirk, S.L. & Karlik, S.J. VEGF and vascular changes in chronic neuroinflammation. *J. Autoimmun.* **21**, 353–363 (2003).
21. Holley, J.E., Newcombe, J., Whatmore, J.L. & Gutowski, N.J. Increased blood vessel density and endothelial cell proliferation in multiple sclerosis cerebral white matter. *Neurosci. Lett.* **470**, 65–70 (2010).
22. Uesugi, N., Muramatsu, R. & Yamashita, T. Endothelin promotes neurite elongation by a mechanism dependent on c-Jun N-terminal kinase. *Biochem. Biophys. Res. Commun.* **383**, 509–512 (2009).
23. Snider, W.D., Zhou, F.Q., Zhong, J. & Markus, A. Signaling the pathway to regeneration. *Neuron* **35**, 13–16 (2002).
24. Hannila, S.S. & Filbin, M.T. The role of cyclic AMP signaling in promoting axonal regeneration after spinal cord injury. *Exp. Neurol.* **209**, 321–332 (2008).
25. Jung, S., Donhauser, T., Toyka, K.V. & Hartung, H.P. Propentofylline and iloprost suppress the production of TNF-α by macrophages but fail to ameliorate experimental autoimmune encephalomyelitis in Lewis rats. *J. Autoimmun.* **10**, 519–529 (1997).
26. Makita, T., Sucov, H.M., Gariepy, C.E., Yanagisawa, M. & Ginty, D.D. Endothelins are vascular-derived axonal guidance cues for developing sympathetic neurons. *Nature* **452**, 759–763 (2008).
27. Dray, C., Rougon, G. & Debarbieux, F. Quantitative analysis by *in vivo* imaging of the dynamics of vascular and axonal networks in injured mouse spinal cord. *Proc. Natl. Acad. Sci. USA* **106**, 9459–9464 (2009).

ONLINE METHODS

Mice. SJL/J mice were obtained from Charles River Japan. All experimental procedures were approved by the Institutional Animal Care and Use Committee of Osaka University.

Induction of a targeted EAE lesion. Adult female SJL/J mice (6–8 weeks old) were subcutaneously immunized with an emulsion of 50 μg bovine MBP (Wako) in complete Freund's adjuvant (Difco) containing 500 μg *Mycobacterium tuberculosis* H37Ra (Difco) on day 0. This immunization protocol alone rarely induces disseminated disease; the few mice in which dissemination occurred after this protocol were excluded from experiment. After 21–23 d, we performed a dorsal laminectomy at Th3–Th4 and injected 1 μl of a cytokine mixture composed of 250 ng recombinant mouse tumor necrosis factor α (TNF-α) (R&D) and 150 U recombinant mouse interferon γ (IFN-γ) (R&D) dissolved in PBS over a 3-min period (CST coordinate: 0.5 mm depth at the midline) into the dorsal column of the thoracic spinal cord. Mice received an intravenous injection of 200 ng pertussis toxin (List Biological Laboratories) in 100 μl PBS on the same day and at 48 h after the injection of TNF-α and IFN-γ.

EAE scores. Individual mice were scored for disease severity on the basis of the following scale: 0, no clinical disease; 0.5, piloerection; 1, tail weakness; 1.5, tail paralysis; 2, hindlimb weakness; 3, hindlimb paralysis; 3.5, forelimb weakness; 4, forelimb paralysis; or 5, moribund or death.

Hindlimb placing test. Independent testing of each hindlimb for placement on a tabletop in response to gentle, purely tactile or proprioceptive (with joint movement) stimulation applied to the front or top of the hindfoot was conducted. Each test was repeated for each hindlimb up to six times or until three correct responses were obtained. The number of completed placing responses (maximum, three) for each hindlimb was noted, and the results for both hindlimbs were added to obtain a hindlimb placing score (minimum, zero; maximum, six)[8].

Histology and immunohistochemistry. At 0, 7, 14, and 28 d after induction of targeted EAE, mice were transcardially perfused with 4% paraformaldehyde (PFA) in PBS. Spinal cord and brain tissues were post-fixed with 4% PFA in PBS at 4 °C overnight, immersed in 30% sucrose in PBS and then embedded in optimal cutting temperature compound (Tissue-Tek) for frozen sectioning. Cross-sections were cut at 20-μm thickness on a cryostat and mounted on Matsunami adhesive silane-coated slides (Matsunami Glass). For histology, sections were stained with H&E (Wako).

For immunohistochemistry, sections were permeabilized in PBS containing 0.1% Triton X-100 and 0.5% BSA for 1 h at room temperature. The sections were then incubated with primary antibodies overnight at 4 °C and then incubated with fluorescently labeled secondary antibody for 3 h at room temperature. The primary antibodies used were as follows: rabbit prostaglandin I synthase (1:100, 100023, Cayman), rabbit IP receptor (1:100, 160070, Cayman), rabbit NeuN (1:100, MAB377, Covance), rabbit amyloid β (A4) precursor protein (APP) (1:100, A8718, Sigma), mouse GFAP (1:100, G3893, Sigma), rat PDGF receptor-α (1:100, 558774, BD Pharmingen), rabbit CD31 (1:100, ab28364, Abcam), rat CD105 (1:50, endoglin; 550546, BD Bioscience), rabbit cox2 (1:100, 160106, Cayman), mouse Ki67 (1:100, 556003, BD Bioscience), rabbit PKC-γ (1:100, sc-211, Santa Cruz), rat CD4 (1:100, 550278, BD Bioscience) and rat CD11b (1:100, 550282, BD Bioscience) antibodies. Alexa Fluor 488- or 568-conjugated goat antibody to rabbit IgG, goat antibody to rat IgG and goat antibody to mouse IgG (Invitrogen) were used as secondary antibodies. The mouse on mouse (MOM) kit (Vector) was used for Ki67 immunohistochemistry.

To estimate the length of vessels, the sections were immunostained with either CD105-specific or CD31-specific antibodies. The length of the vessels in the gray matter was measured in the sections around the targeted EAE lesion (segments Th3–Th4, just rostral to the lesion center). The means were calculated from 5–7 sections spaced 100 μm apart[28].

To assess demyelination in the spinal cord, we performed myelin staining by using a green fluorescent lipophilic dye (FluoroMyelin, Invitrogen) according to the manufacturer's instructions.

Axonal tract tracing. The hindlimb CST was labeled with a 10% solution of BDA (10,000 MW; Invitrogen). BDA was slowly injected into the hindlimb area of the motor cortex (coordinates from bregma: 2.0 mm posterior/2.0 mm lateral, 2.0 mm posterior/2.5 mm lateral, 2.5 mm posterior/2.0 mm lateral and 2.0 mm posterior/2.5 mm lateral, 0.4 μl per site, all at a depth of 0.8 mm into cortex) using a glass capillary attached to a microsyringe. Two weeks after the BDA injections, mice were transcardially perfused with 4% PFA in PBS. The sections of the spinal cord were cut horizontally at 20-μm thickness on a cryostat and mounted on Matsunami adhesive silane-coated slides. For visualizing the BDA, the sections were incubated in PBS containing 0.3% Triton X-100 for 1 h, followed by incubation with Alexa Fluor 488–conjugated streptavidin (1:500, Invitrogen) for 2 h at room temperature.

To quantify the number of sprouting axons, the number of CST collaterals crossing the line positioned in the gray matter was measured as previously reported[29]. We drew a horizontal line through the central canal and across the lateral rim of the gray matter. Two vertical lines were drawn to divide the horizontal line into two equal parts, starting from the central canal to the lateral rim. Only fibers crossing the two lines were counted in each section. To correct for variations in tracing efficiency, the number of CST collaterals per section were normalized to the total number of labeled CST axons on each side; 4–6 sections spaced 100 μm apart were examined. The average number of CST collaterals per section was divided by the number of labeled CST fibers and multiplied by the number of CST fibers at the level of the medulla[30].

Propriospinal neurons were labeled with Alexa Fluor 555–conjugated CTB (Invitrogen). Under anesthesia, half of the L1–L2 vertebrates were laminectomized. The tracer was injected into the exposed spinal cord 200 μm lateral to the midline, 0.4 μl per site, at a depth of 300 μm. At each location, the glass capillary was left in position for an additional 1 min before withdrawal. All the sections were analyzed using a fluorescence (Olympus BX51, DP71) or confocal laser–scanning microscope (Olympus FluoView FV1000). The number of contacts of BDA-labeled axons with Alexa Fluor 555–labeled propriospinal neurons was determined as described[31] in the section around the EAE lesion (segments Th2–Th3, one segment above the lesion center). The average numbers of contacts per section were divided by the number of labeled CST fibers and multiplied by the number of counted CST fibers at the level of medulla. The means were calculated from each of five sections spaced 100 μm apart.

Surgical procedure. For pharmacological treatments in mice, anesthetized female SJL/J mice underwent laminectomy at thoracic level Th3–Th4, and a cannula from the Alzet osmotic minipump (model numbers 1002 and 1004, Alzet Corp) was placed under the dura at the thoracic cord immediately after injection of the cytokine mixture. The osmotic minipump was filled with vehicle solution (saline), CAY10441 (0.31 μg per kg of body weight per d over 2 or 4 weeks) or iloprost (0.36 μg per kg of body weight per d over 2 or 4 weeks), and the pump was placed subcutaneously in the back. To selectively kill spinal cord neurons, the excitotoxic glutamate agonist NMDA (Sigma) was stereotaxically injected into the spinal cord gray matter at Th2–Th3 at a 0.3 μl volume of 1 mM NMDA per site and a depth of 800 μm.

To determine the size of the lesion, we perfused mice transcardially with 4% PFA in PBS 3 d after NMDA injection. Horizontal sections of the spinal cord (30-μm thick) were taken at 150-μm intervals, including the site of NMDA injection. The sections were stained with NeuroTrace red fluorescent Nissl stain (Invitrogen). We assessed the length of the lesion in the longitudinal direction by analyzing the area of cell loss in each section.

Preparation and transfection of siRNA. Mouse IP receptor siRNA and PGIS siRNA were synthesized by Invitrogen (Stealth siRNA). The sense and antisense strands of siRNA were as follows: IP receptor siRNA1, 5′-GAAAGGCUGUC UUCCAACGCCUCAA-3′ (sense) and 5′-UUGAGGCGUUGGAAGACAGC CUUUC-3′ (antisense); IP receptor siRNA2, 5′-UCUCGGGCACGAGAGGA UGAAGUUU-3′ (sense) and 5′-AAACUUCAUCCUCUCGIGCCCGAGA-3′ (antisense); PGIS siRNA1, 5′-GGGAAGAGUUAUGCCAUCAACAGCA-3′ (sense) and 5′-UGCUGCCGAUGGCAUAACUCUUCCC-3′ (antisense); PGIS siRNA2, 5′-GGGAGAGAUGCUGCCAGCUUCCUUA-3′ (sense) and 5′-UAAG GAAGCUGGCAGCAUCUCUCCC-3′ (antisense). The 5′ ends of these siRNAs were labeled with Alexa Fluor 555. Transfection of the IP receptor siRNA with

cultured cortical neurons was performed using the Nucleofector transfection device (Amaxa) according to the manufacturer's protocols.

Transfection of PGIS siRNA with cultured endothelial cells was performed using Lipofectamine 2000 (Invitrogen). The cells were lysed 72 h after transfection and then subjected to western blot analysis.

For *in vivo* experiments, aliquots of the stock solution were mixed with i-Fect transfection reagent (Neuromics). The mice received intracortical injections (2 μg siRNA μl^{-1}; coordinates from bregma: 2.0 mm posterior/2.0 mm lateral, 2.0 mm posterior/2.5 mm lateral, 2.5 mm posterior/2.0 mm lateral and 2.0 mm posterior/2.5 mm lateral, all at a depth of 0.8 mm into cortex) of either a lipid-encapsulated IP receptor–selective siRNA or i-Fect–encapsulated nontargeting double-stranded RNA (dsRNA) (control mismatch siRNA) on days 0 and 14 after induction of targeted EAE. BDA was simultaneously injected in the mixture with the siRNAs. Injection of siRNA or the transfection reagents alone into motor cortex did not cause any signs of toxicity at the behavioral level assessed in open-field test (data not shown).

For knockdown of PGIS in vascular endothelial cells *in vivo*, PGIS siRNA or nontargeting dsRNA in saline (50 μg siRNA ml^{-1}) was rapidly injected within 5–10 s into the mouse tail vein on days 0, 7 and 14 after induction of targeted EAE. This procedure was previously shown to achieve selective gene transfer to vascular endothelial cells[32]. Injection of either the siRNA or saline alone into the vein did not result in any signs of toxicity, as assessed by behavior (data not shown).

Western blot analysis. The tissues or cells were homogenized in 10 mM Tris-HCl (pH 7.4), 150 mM NaCl, 1% Triton X-100 and 1 mM EDTA containing protease inhibitor (Roche). The lysates were clarified by centrifugation at 13,000*g* at 4 °C for 20 min, and the supernatants were collected and normalized for protein concentration. Proteins were separated by 8% SDS-PAGE and transferred onto polyvinylidene difluoride membranes (Immobilon-P, Millipore). After blocking with PBS containing 5% skim milk and 0.05% Tween 20, the membranes were incubated with primary antibodies.

For detection, a fluorescence-conjugated secondary antibody and an electrogenerated chemiluminescence system (GE Healthcare) were used. The membrane was exposed to an imaging system (LAS-3000, Fujifilm) according to the manufacturer's specifications. The protein bands were quantified using ImageJ software. The following antibodies were used: mouse α-tubulin (1:1,000, sc-5286, Santa Cruz), rabbit antibodies to prostaglandin I synthase (1:1,000, 100023, Cayman) and rabbit antibodies to IP receptor (1:1,000, 160070, Cayman). Horseradish peroxidase–conjugated mouse IgG–specific and rabbit IgG–specific antibodies were used as secondary antibodies (1:5,000, Cell Signaling Technology).

Primary culture of cortical neurons. Cortical neurons used for primary cultures were prepared from cerebral cortices obtained from mice at postnatal day 1. The cerebral cortices were dissociated by trypsinization (treatment with 0.25% trypsin in PBS for 15 min at 37 °C) followed by resuspension in DMEM containing 10% (v/v) heat-inactivated FBS (Gibco) and trituration. For the neurite outgrowth assay, the isolated cells were plated on culture dishes coated with 0.1 mg ml^{-1} collagen type IV (Sigma) and 0.1 mg ml^{-1} fibronectin (Sigma) at a density of 1–2 × 10^4 cells per cm^2 in DMEM supplemented with 2% (v/v) B27 (Invitrogen). After culturing for 24 h, cells were immunostained with mouse β-tubulin–specific (Tuj1; 1:100, MMS-425P, Covance) and rat Ctip2-specific (1:1,000, ab18465, Abcam) antibodies to measure the neurite length of subcortical projection neurons. The following pharmacological reagents were used in the cultures: 100 μM Sp-cAMPS (Sigma) and 100 μM Rp-cAMPS (Sigma). To analyze the effect of prostacyclin, 1 μM CAY10441 (Cayman) and 1 μM iloprost (Cayman) were used. All the reagents were added to the cortical neuron cultures 30 min before the start of the coculture assay.

Primary culture of endothelial cells. Primary cultures of mouse brain capillary endothelial cells were prepared from 3-week-old female SJL/J mice. Mouse cerebral cortices and spinal cords, free of meninges, were digested in a mixture of 1 mg ml^{-1} collagenase type 2 (Worthington) and 6.7 μg ml^{-1} DNase (Sigma) in DMEM for 1.5 h at 37 °C. The cell pellet was separated by centrifugation in 20% BSA-DMEM (1,000*g*, 10 min) and then incubated for another 45 min at 37 °C with a mixture of 1 mg ml^{-1} collagenase-dispase (Roche) and 6.7 μg ml^{-1} DNase in DMEM at 37 °C. Microvessel endothelial cell clusters were separated on a 33% continuous Percoll gradient (GE Healthcare), collected and plated on culture dishes coated with 0.1 mg ml^{-1} collagen type IV and 0.1 mg ml^{-1} fibronectin. Endothelial cells were grown in DMEM supplemented with 10% (v/v) heat-inactivated FBS, 1 mM 4-(2-hydroxyethyl)-1-piperazineethanesulfonic acid (HEPES), 2 mM glutamine (Gibco), 2 ng ml^{-1} basic fibroblast growth factor (bFGF) (R&D) and 4 μM hydrocortisone (Sigma); in addition, the medium was supplemented with 1 μg ml^{-1} puromycin (Sigma). The absence of contamination in the endothelial cell culture was confirmed by immunostaining with the endothelial cell marker CD31. For the coculture experiments, cortical neurons and endothelial cells were grown separately on the lower wells and upper chambers of a transwell coculture system, respectively.

Cortical evoked CDPs. The sensory motor cortex and lumber spinal cord were exposed in mice anesthetized with ketamine hydrochloride (100 mg per kg of body weight, intraperitoneally (i.p.)) and xylazine hydrochloride (5 mg per kg of body weight, i.p.). Cortical evoked potentials were elicited by electrical stimulation (10 square-wave pulses at 330 Hz, 50 μA, 200 ms; STG4002, Multichannel Systems) of the left sensory motor cortex using 50-μm–diameter Teflon-coated tungsten wires (A-M systems) lowered 0.8 mm into the cortex. Postsynaptic potentials evoked by the cortical stimuli were recorded with a silver ball electrode placed medially on the contralateral cord surface using a PowerLab (AD Instruments). At each recording site (L1–L2), 20 responses were averaged and stored for off-line analysis of amplitude and latency.

T cell proliferation and cytokine analysis. Spleens were harvested from control-, iloprost- and CAY10441-treated EAE mice on day 7. Freshly isolated spleen was prepared and treated with ammonium-chloride-potassium (ACK) lysing buffer (Lonza) to remove erythrocytes. The cell suspension was filtered through a fine mesh screen. Single cells were plated at a density of 5 × 10^6 cells ml^{-1} in RPMI 1640 medium supplemented with glutamine (Gibco), sodium pyruvate, penicillin, streptomycin, 2-mercaptoethanol (Wako) and 10% FBS. To re-stimulate the T cells, 50 μg ml^{-1} MBP was initially added to the culture. After stimulation for 24 h, cell proliferation was estimated by the measurement of BrdU incorporation into newly synthesized cellular DNA using the Cell Proliferation ELISA and BrdU (colorimetric) kit (Roche) according to the manufacturer's instructions. To measure the production of cytokines, the splenocytes obtained from mice with EAE were cultured with 50 μg ml^{-1} MBP peptide. After stimulation for 72 h, supernatants were collected, and the expression of a panel of cytokines was measured using the Q-Plex Mouse Cytokine Array (Quansys Biosciences) according to the manufacturer's instructions. To measure cytokine expression in the spinal cord, tissues were homogenized in 10 mM Tris-HCl (pH 7.4), 150 mM NaCl, 1% Triton X-100 and 1 mM EDTA containing protease inhibitor. Samples were centrifuged at 15,000*g* for 20 min at 4 °C. The supernatant was aliquoted and stored at −80 °C. The expression of a panel of cytokines was measured using the Q-Plex Mouse Cytokine Array (Quansys Biosciences) according to the manufacturer's instructions.

Enzyme immunoassay. PGI_2 synthesis in cell culture and spinal cord tissue was assessed by quantifying its stable metabolite (6-keto–PGF1-α; Cayman) according to the manufacturer's instructions. To measure 6-keto–PGF1-α expression in the spinal cord, tissues were homogenized in 137 mM NaCl, 20 mM Tris-HCl (pH 8.0), 1% NP-40, 10% glycerol and protease inhibitor. The lysates were clarified by centrifugation at 13,000*g* at 4 °C for 20 min, and the supernatants were collected and normalized for protein concentration. To measure 6-keto–PGF1-α expression in conditioned media, vascular endothelial cells were plated at a density of 5 × 10^5 cells ml^{-1} in DMEM supplemented with 10% (v/v) heat-inactivated FBS, 1 mM HEPES, 2 mM glutamine, 2 ng/ml bFGF and 4 μM hydrocortisone. After 1 d in culture, the culture supernatant was collected and stored at −20 °C.

Immunohistochemical staining of human tissues. We obtained autopsied spinal cord tissues from three individuals with relapsing-remitting multiple sclerosis. We formalin fixed the spinal cord samples, embedded them in paraffin and cut them into 4-μm–thick sections for immunohistochemistry.

We then deparaffinized, washed and subjected the sections to an antigen-retrieval procedure by heating the sections in citrate buffer. We incubated tissue samples with primary antibodies specific for human CD105 (1:10, M352701, Dako) and PGIS (1:100, 160640, Cayman) and Alexa Fluor 488– or 568–conjugated goat mouse IgG and goat rabbit IgG (Invitrogen) secondary antibodies. The research protocol was approved by the Human Use Review Committees of the Graduate School of Medicine, Osaka University, and Toneyama National Hospital, for the Protection of Human Subjects. Informed consent was obtained from all subjects.

Statistical analyses. Data are presented as mean ± s.e.m. For clinical scores, significance between groups was examined using Bonferroni's test. Other statistics were analyzed using either an unpaired Student's *t* test, repeated measures ANOVA or one-way ANOVA followed by Scheffe's tests or Tukey's tests. $P < 0.05$ was considered to be significant.

28. Tammela, T. *et al.* Blocking VEGFR-3 suppresses angiogenic sprouting and vascular network formation. *Nature* **454**, 656–660 (2008).
29. Vavrek, R., Girgis, J., Tetzlaff, W., Hiebert, G.W. & Fouad, K. BDNF promotes connections of corticospinal neurons onto spared descending interneurons in spinal injured rats. *Brain* **129**, 1534–1545 (2006).
30. Liu, K. *et al.* PTEN deletion enhances the regenerative ability of adult corticospinal neurons. *Nat. Neurosci.* **13**, 1075–1081 (2010).
31. Ueno, M., Hayano, Y., Nakagawa, H. & Yamashita, T. Intraspinal rewiring of the corticospinal tract requires target-derived neurotrophic factor and compensates lost function after brain injury. *Brain* **135**, 1253–1267 (2012).
32. Hino, T. *et al. In vivo* delivery of small interfering RNA targeting brain capillary endothelial cells. *Biochem. Biophys. Res. Commun.* **340**, 263–267 (2006).